Journal of Biomolecular NMR, **21:** 209–220, 2001.
KLUWER/ESCOM

The Solution Structure of [d(CGC)r($a_m a_m a_m$)d(TTTGCG)]$_2$

Ya-Ping Tsao[a,*], Lian-Yong Wang[b,*], Shang-Te Hsu[a], Moti L. Jain[a], Shan-Ho Chou[c], Wen-Chang Huang[b,*] & Jya-Wei Cheng[a,**]
[a]*Division of Structural Biology and Biomedical Science, Department of Life Science, National Tsing Hua University, Hsinchu 300, Taiwan, Republic of China*
[b]*Department of Chemistry, National Taiwan Normal University, Taipei, Taiwan, Republic of China*
[c]*Institute of Biochemistry, National Chung Hsing University, Taichung 400, Taiwan, Republic of China*

Received 7 June 2001; Accepted 27 August 2001

Key words: 2′-OMe RNA, DNA•RNA, NMR, solution structure

Abstract

The solution structure and hydration of a DNA•RNA hybrid chimeric duplex [d(CGC)r($a_m a_m a_m$)d(TTTGCG)]$_2$ in which the RNA adenines were substituted by 2′-O-methylated riboadenines was determined using two-dimensional NMR, simulated annealing, and restrained molecular dynamics. Only DNA residue 7T in the 2′-OMe-RNA•DNA junction adopted an O4′-endo sugar conformation, while the other DNA residues including 3C in the DNA•2′-OMe-RNA junction, adopted C1′-exo or C2′-endo conformations. The observed NOE intensity of 2′-O-methyl group to H1′ proton of $4a_m$ at the DNA•2′-OMe-RNA junction is much weaker than those of $5a_m$ and $6a_m$. The 2′-O-methyl group of $4a_m$ was found to orient towards the minor groove in the trans domain while the 2′-O- methyl groups of $5a_m$ and $6a_m$ were found to be in the gauche (+) domain. In contrast to the long-lived water molecules found close to the RNA adenine H2 and H1′ protons and the methyl group of 7T in the RNA-DNA junction of [d(CGC)r(aaa)d(TTTGCG)]$_2$, there were no long-lived water molecules found in [d(CGC)r($a_m a_m a_m$)d(TTTGCG)]$_2$. This is probably due to the hydrophobic enviroment created by the 2′-O-methylated riboadenines in the minor groove or due to the wider minor groove width in the middle of the structure. In addition, the 2′-O-methylation of riboadenines in pure chimeric duplex increses its melting temperature from 48.5 °C to 51.9 °C. The characteristic structural features and hydration patterns of this chimeric duplex provide a molecular basis for further therapeutic applications of DNA•RNA hybrid and chimeric duplexes with 2′-modified RNA residues.

Introduction

The structure and recognition of DNA•RNA hybrid duplexes and DNA•RNA chimeric duplexes have been the focus of numerous studies because of their crucial roles in transcription, reverse transcription, and replication (Ban et al., 1994; Chou et al., 1989; Gonzalez et al., 1994; Gyi et al., 1998; Hall and McLaughlin, 1991; Hashem et al., 1998; Jaishree et al., 1993; Nishizaki et al., 1996; Ratmeyer et al., 1994; Rice and Gao, 1997; Wang et al., 1982). In addition, it is well known that incorporation of 2′-O-methylated RNA residues can increase the thermal stability and inhibit RNase H hydrolysis of DNA•RNA hybrid and chimeric duplexes (Nishizaki et al., 1997; Tereshko et al., 1998). Significant efforts have been made thereafter on the structural studies of 2′-O-modified RNA analogues into the DNA•RNA hybrid and chimeric duplexes owing to their potential therapeutic applications such as antisense agents and enzyme inhibitors (Egli and Gryaznov, 2000).

X-ray crystallographic studies have found that even the introduction of one 2′-O-methylated ribonucleotide into the DNA strand transforms the whole duplex to the A-form geometry with all the sugars

*The first two authors should be regarded as joint First Authors.
**Authors to whom correspondence should be addressed. E-mails: jscjw@life.nthu.edu.tw; huangwc@cc.ntnu.edu.tw

in the C3′-endo conformation and the 2′-O-methyl groups directed into the minor groove (Lubini et al., 1994; Tereshko et al., 1998). The increased stability of the DNA•RNA chimeric duplex was attributed to the hydrophobic interactions between substituents in the minor groove (Lubini et al., 1994). Similar results have been found for NMR structural studies of (ggagaugac)·($g_mu_mc_mATCTc_mc_m$) (Nishizaki et al., 1997), where lowercase letters, capital letters, and lowercase letters with the subscript m are RNA, DNA, and 2′-O-methylated RNA. The overall structure of (ggagaugac)·($g_mu_mc_mATCTc_mc_m$) was close to the typical A-form duplex with sugars having C3′-endo conformations and the 2′-O-methyl groups pointing into the minor groove with the torsion angles in the gauche(+) domain (Nishizaki et al., 1997).

On the other hand, NMR studies have revealed that for (GCGTTGCG)·($g_mg_mc_ma_ma_mc_mc_mc_m$), the sugars of the 2′-O-methylated RNA residues are in the C3′-endo conformation but the sugars of the complementary DNA strand are mainly in the C2′-endo conformation (Blommers et al., 1994). Similar heteromerous structure in which the sugars of the RNA strand have the normal N-type C3′-endo conformation, but the sugars of the DNA strand have the intermediate O4′-endo conformation, have been observed for pure DNA•RNA hybrid duplexes by NMR (Gonzalez et al., 1994, 1995; Gyi et al., 1998; Salazar et al., 1993b). The minor groove width of pure DNA•RNA hybrid duplexes was found to be between that of A- and B-form duplexes (Fedoroff et al., 1993). These structural features were used to explain the mechanism whereby RNase H discriminates between DNA•RNA hybrid duplexes and pure RNA or DNA duplexes (Fedoroff et al., 1993).

Previously, we have determined the solution structure and hydration of the chimeric duplex $[d(CGC)r(aaa)d(TTTGCG)]_2$ (Hsu et al., 2000a, b). The solution structure of this chimeric duplex differs from the previously determined X-ray structure of the analogous B-DNA duplex $[d(CGCAAATTTGCG)]_2$ (Edwards et al., 1992) as well as NMR structure of the analogous A-RNA duplex $[r(cgcaaauuugcg)]_2$ (Conte et al., 1997). The long-lived water molecules with correlation time τ_c larger than 0.3 ns were found close to the RNA adenine H2 and H1′ protons in the hybrid segment. A long-lived water molecule was also detected close to the methyl group of 7T in the RNA-DNA junction but not with the other two thymines (8T and 9T). Only DNA residue 7T in the RNA-DNA junction adopted an O4′-endo sugar conformation, while the other DNA residues including 3C in the DNA-RNA junction, adopted C1′-exo or C2′-endo conformations. The minor groove width of $[d(CGC)r(aaa)d(TTTGCG)]_2$ is wider than its B-DNA analog but narrower than that of the A-RNA analog. These distinct structural features and hydration patterns of the chimeric duplex provide a molecular basis for further understanding the structure and recognition of DNA•RNA hybrid and chimeric duplexes.

Recently, Kochetkov and co-workers have found that RNA/DNA chimeras can be used as templates for HIV-1 reverse transcriptase (Gudima et al., 1997). Hogrefe et al. have reported that DNA•RNA hybrid flanked by DNA duplexes can be recognized by *E. coli* RNase H (Hogrefe et al., 1990). Also, it has been proposed that RT-associated RNaseH domain, which degrades the RNA template of DNA•RNA hybrid chimeric duplexes, may distinguish double-strand RNA, RNA•DNA junctions and hybrid duplexes according to their distinct hydration patterns (Szyperski et al., 1999). In the present manuscript we describe the solution structure of a DNA•RNA chimeric duplex $[d(CGC)r(a_ma_ma_m)d(TTTGCG)]_2$ in which the RNA residues are substituted by 2′-O-methylated riboadenines. The possible correlation between the structure and functional properties of this chimeric duplex may have potential therapeutic applications with the important enzymes such as HIV reverse transcriptase and RNase H.

Materials and methods

Sample preparations

The $d(CGC)r(a_ma_ma_m)d(TTTGCG)$ dodecamer was prepared on an Applied Biosystems 380B DNA synthesizer in 6 μmol scale using solid-phase phosphoramidite chemistry (Chou et al., 1989). The purified sample (15 mg) was dissolved in 0.3 ml of 90%H_2O:10%D_2O containing 20 mM sodium phosphate, 200 mM sodium chloride and 0.05 mM EDTA, at pH 7.0. For non-exchangeable proton studies, the sample was repeatedly dried from 99.96% D_2O in a speed vacuum, and then dissolved in 0.3 ml of 99.996% D_2O.

NMR spectroscopy

NMR data were recorded on a Bruker Avance 600 MHz NMR spectrometer equipped with a triple-resonance three-axis gradient probe. The phase sensi-

tive NOESY and ROESY spectra in water (containing 10%D_2O) were recorded at 273, 278, 283 and 300 K under identical conditions except at different mixing times of 50 and 100 ms, respectively. The intense bulky water signal was suppressed using the Watergate method (Piotto et al., 1992) with a short delay τ of 139 μs, resulting the optimum excitation near 1.7, 7.7, and 13.7 ppm. These spectra were collected into 2048 complex points in the t_2 dimension and 800 complex points in the t_1 dimensions with relaxation delay of 1.4 second between each scan. These data were further apodized with a sin-square window function and zero-filled to 4096 complex points in the t_2 dimension and 1024 complex points in the t_1 dimension. For nonexchangable protons, NOESY spectra at four different mixing times of 60, 120, 240 and 480 ms were acquired during a 4-day period without removing the sample from the probe at 303 K. These phase-sensitive NOESY spectra were collected into 2048 complex points in the t_2 dimension and 512 points in the t_l dimension with 32 scans per t_l experiment and a relaxation delay of 5 seconds between each scan (Wang et al., 1992). The acquired data were transferred to an IRIS Indigo 2 workstation and processed using the XWIN-NMR program (Bruker). The NOESY data sets were apodized with a shifted-sinebell window function for the first 512 points and zero filled to 2048 points in both the t_2 and t_l dimensions. The DQF-COSY spectrum was recorded in the phase-sensitive mode with time-proportional phase incrementation.

Distance restraint determinations

The proton-proton distances were calculated using the NOE initial rate two-spin approximation at short mixing times normalized to the cross-relaxation rate of the cytosine H5-H6 proton pairs in NOESY spectra collected in D_2O (d_{H5-H6} = 2.5 Å) (Noggle and Schirmer, 1971). To guard against spin-diffusion, we initially used the qualitative NOE pattern to establish that this duplex is in the broad family of right-handed structures, and then used this information to ascertain which spin pairs are likely to have an intervening third spin that might produce errors in the calculated distance (Cheng et al., 1992). For non-exchangeable protons, typical error limits for the upper and lower bound restraints were ±0.4 Å for distances less than 3 Å, ±0.8 Å for distances less than 4 Å, and ±1.4 Å for distances greater than 4 Å. For exchangeable protons, the distance restraints were set loosely to 2–4 Å for strong cross-peaks and 3–6 Å for weak cross-peaks in NOESY spectra collected in water. Based on the averaged hydrogen bond length derived from structure coordinates of twenty DNA, RNA, and DNA•RNA hybrid duplexes (PDB code: 124d, 161d, 1al5, 1d65, 1d87, 1d88, 1d96, 1dpl, 1dpn, 1efs, 1evp, 1gtc, 1nao, 1pbm, 1pbl, 259d, 310d, 398d, 410d, 461d), the hydrogen bond restraints were defined as following: A(N6)-T(O4) = 2.94 ± 0.20 Å, A(N1)-T(N3) = 2.82 ± 0.20 Å , G(N1)-C(N3) = 2.95 ± 0.20 Å, G(N2)-C(O2) = 2.86 ± 0.20 Å, G(O6)-C(N4) = 2.95 ± 0.20 Å.

Sugar and backbone conformations

To maintain a right-handed helix structure between A- and B-form conformation, six backbone dihedral angles restraints ($\alpha = -65° \pm 60°$, $\beta = 170° \pm 60°$, $\gamma = 55° \pm 60°$, $\delta = 115° \pm 60°$ for DNA and $90° \pm 60°$ for RNA residues, $\varepsilon = 180° \pm 60°$ and $\zeta = -75° \pm 60°$) were employed for each residue to exclude unreasonable geometry. The sugar and backbone conformation of the individual residue was further confirmed via a combination of NOESY distances and *J*-coupling data, as outlined by Reid and co-workers (Kim et al., 1991; Salazar et al., 1993a). This combined strategy to constrain the backbone was used for other DNA•RNA chimeras (Fedoroff et al., 1996; Hsu et al., 2000a; Nishizaki et al., 1996; Salazar et al., 1996, 1994; Zhu et al., 1995) and described in more detail elsewhere (Cheng et al., 1992; Kim et al., 1991). In addition, two sugar pucker dihedral angle restraints (from a combination of NOESY and DQF-COSY data) and one χ angle restraint were also added to maintain the B-type and A-type sugar conformation for DNA and RNA residues, respectively.

Structure calculations and analysis

Three-dimensional structures of [d(CGC)r($a_m a_m a_m$) d(TTTGCG)]$_2$ were calculated using 454 NOE distance restraints, 30 hydrogen bond restraints, and 208 backbone, sugar, and glycosidic dihedral angle restraints. Distance restraints were derived from 258 intranucleotide, 142 sequential, 4 cross-strand, and 50 exchangeable proton NOEs. Initial A- and B-form DNA• 2′-O-methylated-RNA chimeric structures were generated using Insight II (Molecular Simulations Inc.) program. First, the simulated annealing protocol in the program X-PLOR 3.851 (A.T. Brünger, Yale University) was applied to the starting structures at 1000 K and slowly cooled to 300 K with a time step

Table 1. Structure statistics for the 10 final refined structures of $[d(CGC)r(a_m a_m a_m)d(TTTGCG)]_2$

NOE restraints	454
Intranucleotide[a]	258
Sequential[a]	142
Interstrand	4
Involving exchange protons	50
Torsion angle restraints[b]	208
Hydrogen bond restraints	60
Relaxation matrix refinement	
Number of peak integrals used at each mixing time[c]	250
Average $R^{1/6}$ factor	0.0268 ± 0.00026
Refinement statistics (10 final lowest-energy structures)	
NOE violation > 0.5 Å	1
Dihedral angle violation > 5 degree	0
Average pairwise rmsd	
All heavy atom	1.12 ± 0.37
Without 5′ and 3′ terminus	0.82 ± 0.25
Hybrid region[d]	0.31 ± 0.12
Average rmsd from ideal covalent geometry	
Bond lengths (Å)	0.0090 ± 0.0001
Bond angles (degree)	3.906 ± 0.01
Impropers (degree)	0.41 ± 0.002

[a]The NOE restraints were for the two degenerate strands.
[b]See Materials and methods.
[c]Cross-peak volumes were measured in three NOESY spectra with mixing times of 60, 120, and 240 ms. Number of peaks were for the two degenerate strands.
[d]Hybrid segment is defined as $4a_m$ to 9T, i.e., $[r(a_m a_m a_m)d(TTT)]_2$.

of 1.5 ps per 50 K. From the 50 simulated annealing structures, ten structures with the lowest energy were chosen for further optimization. Restrained molecular dynamic was then carried out in vacuum with a distance-dependent dielectric constant. The dynamics was initiated at 300 K and the temperature was gradually increased to 1000 K with a time step of 0.5 ps per 50 K and then evolved for 20 ps at 1000 K. Subsequently, the system was cooled down to 300 K in 14 ps and equilibrated for 9 ps. The coordinates saved after every 0.5 ps in the last 2.0 ps of the equilibrium were averaged, and the averaged structure was subjected to a further conjugate gradient minimization of 500 steps using Powell algorithm until a final gradient of 0.1 kcal mol^{-1} was reached. All the structures were finally refined by relaxation matrix based on NOE intensity (Yip & Case, 1989). NOE volumes of 125 cross-peaks were integrated for each NOESY spectrum at three different mixing times (60, 120 and 240 ms) and used as restraints with uniform upper and lower bonds of $\pm 10\%$. These restraints were doubled to 250 for two degenerate strands. With the incorporation of distance and dihedral restraints, the $R^{1/6}$ factor (Nilges et al., 1991; White et al., 1992) was minimized during the refinement. A cutoff of 5.5 Å was applied for relaxation calculation and an isotropic correlation time of 5.0 ns was used based on a grid search. During dynamics, the temperature of the system was slowly heated from 100 K to 1000 K as the force constant of relaxation was scale up to a final value of 400. Simultaneously, the force constants of distance restraints of non-exchangeable protons were scaled down to zero. The system was then cooled down to 300 K and the final structure was subjected to conjugate gradient minimization until a final gradient of 0.1 kcal mol^{-1} was reached. The hydrogen bonding of base pairing and exchangeable proton distance restraints were maintained throughout the refinement.

Ten final refined structures were selected for further structural analysis. The helical parameters and torsion angles were analyzed by CURVE 5.2 (Lavery and Sklenar, 1989). The family of 10 structures, together with the NMR restraints used in their determination, has been deposited with the Protein Data

Table 2. Rmsd values between different structures (Å)

Structure	a3T3-OMe	a3T3	A3T3	A3U3	A-DNA	B-DNA	A-RNA
a3T3	4.74 ± 0.29						
A3T3	5.47 ± 0.12	4.22 ± 0.14					
A3U3	3.90 ± 0.11	4.41 ± 0.16	4.82				
A-DNA	4.66 ± 0.18	6.13 ± 0.22	6.55	3.67			
B-DNA	5.70 ± 0.13	4.74 ± 0.28	2.83	5.39	6.50		
A-RNA	4.49 ± 0.13	5.46 ± 0.16	6.12	3.33	1.30	5.98	

[1]Rmsd values were calculated pairwise using the best 10 structures. [2]a3T3-OMe represents [d(CGC)r($a_m a_m a_m$)d(TTTGCG)]$_2$, a3T3 represents [d(CGC)r(aaa)d(TTTGCG)]$_2$, A3T3 represents [d(CGCAAATTTGCG)]$_2$, A3U3 represents [r(cgcaaauuugcg)]$_2$, and A-DNA, B-DNA, A-RNA represent the standard A- and B-form DNA and A-form RNA.

Bank. The chemical shifts have been deposited to the Biomagnetic Resonance Bank at the University of Wisconsin.

Results

Resonance assignments and analysis of NMR data

The numbering system for [d(CGC)r($a_m a_m a_m$)d(TTTGCG)]$_2$ as well as its expanded region of the 2D NOESY spectrum in H_2O recorded at 278 K, 14.1 T is shown in Figure 1. Its exchangeable and non-exchangeable proton cross-peaks were assigned using NOESY, ROESY, and TOCSY spectra. The H1′ protons were assigned by standard sequential assignment method, followed by the assignment of H2′ and H2″ protons of DNA, as well as H3′ and H4′ protons of all residues (Hare et al., 1983; Wuthrich, 1986). The H2′ proton of the three 2′-O-methylated RNA adenines were assigned using the H2′-H3′ cross-peaks in the TOCSY spectrum. All the three 2′-O-methylated RNA adenine H2 protons showed both interresidue and intraresidue cross-peaks, particularly in the H6/H8-H1′ region (Figure 1). No cross-peaks between 2′-O-methylated RNA adenine H2 protons and water along the F2 dimension were detected (Figure 1). In addition to the exchangeable and non-exchangeable proton assignments, we have observed three sets of NOEs from the three 2′-O-methyl groups resonating at 3.5–4.0 ppm to the ribose protons. These chemical shifts are in agreement with previously published assignments of 2′-O-methyl protons (Blommers et al., 1994; Nishizaki et al., 1997). Comparing with the pure DNA•RNA chimeric duplex [d(CGC)r(aaa)d(TTTGCG)]$_2$ (Hsu et al., 2000a), major chemical shift perturbations were found in the central hybrid segment. Significant up-field shifts were found for H2′ protons of 2′-O-methylated RNA adenines and for the methyl groups of thymines (data not shown). The chemical shifts of the exchangeable and non-exchangeable protons of [d(CGC)r($a_m a_m a_m$)d(TITGCG)]$_2$ are provided in the supplementary materials (Table S1).

In the NOESY data collected in D_2O for the H8/H6 to the DNA H2′/H2″ region (data not shown), the (n)H6/H8 to (n)H2′ peaks were the most intense and were stronger than the (n)H6/H8 to (n-1)H2″ peaks, which in turn were uniformly stronger than the (n)H6/H8 to (n)H2″ and (n)H6/H8 to (n-l)H2′ peaks. These results indicate that none of the DNA residue in this chimeric duplex assumes a pure A-form conformation in solution. Furthermore, all the DNA sugar residues have quite respectable H1′-H2′ and H3′-H4′ cross peaks in the DQF-COSY spectrum indicating that sugar conformations for the DNA residues are not A-form (data not shown). The DNA residue 7T in the RNA-DNA junction, however, was found to have medium to strong H2″-H3′ DQF-COSY cross peak (Figure 2). The other DNA residues, including residue 3C in the DNA-RNA junction, showed very weak or no detectable H2″-H3′ cross peaks in the DQF-COSY spectrum. The above results indicate that residue 7T in the 2′-OMe-RNA•DNA junction adopts a sugar conformation close to the O4′-endo, while the other DNA residues adopt C1′-exo or C2′-endo conformations (Hsu et al., 2000a; Salazar et al., 1993a). No detectable H1′-H2′ DQF-COSY cross peaks for 2′-O-methylated RNA adenines were observed. Also, strong (n)H8 to (n-1)H2′ NOESY cross peaks were found for the 2′-O-methylated RNA adenines indicating that the 2′-O-methylated RNA segment in the chimeric strand assumes an A-form conformation.

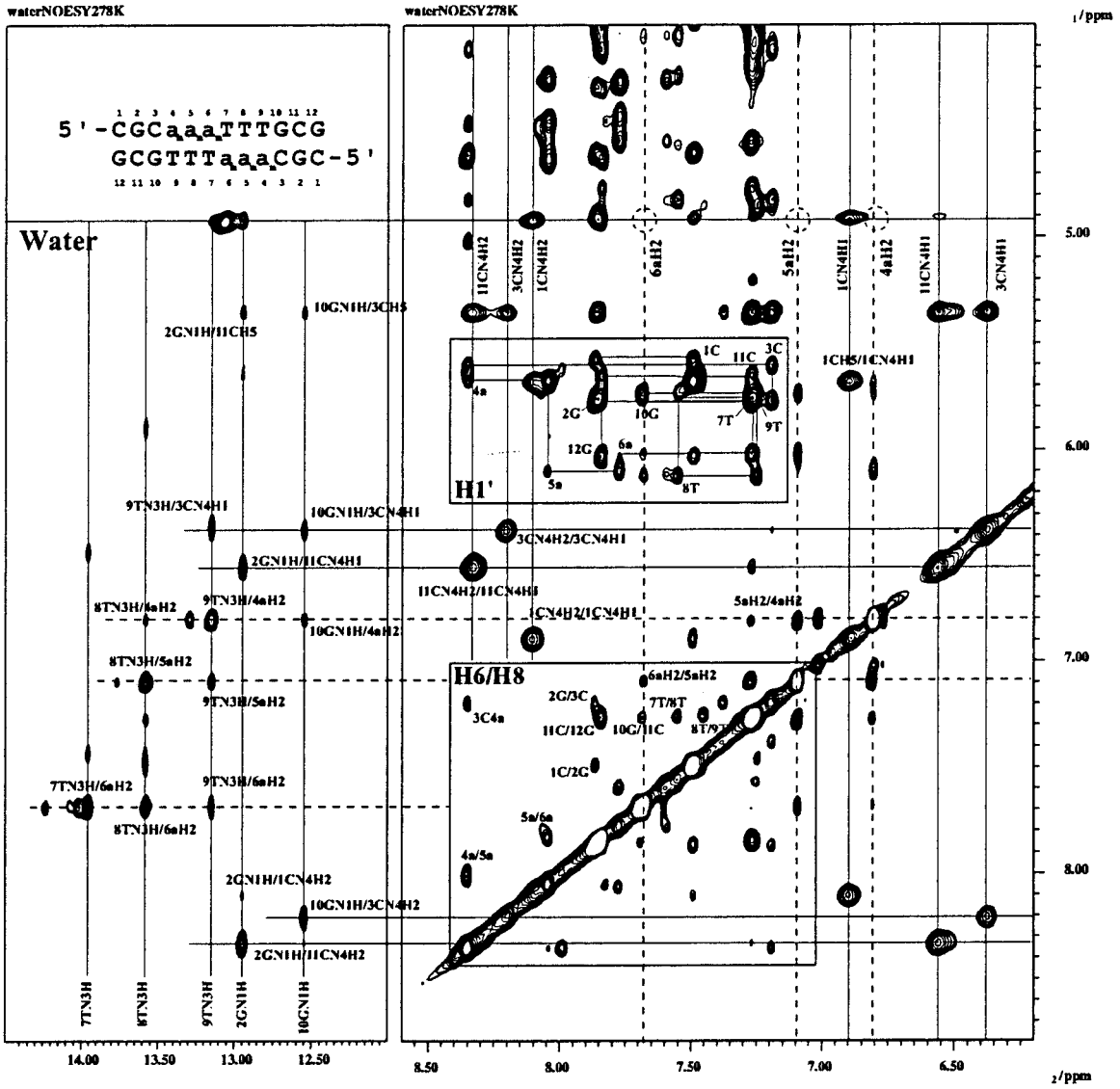

Figure 1. Expansion of the 100 ms water NOESY spectrum of [d(CGC)r($a_m a_m a_m$)d(TTTGCG)]$_2$ at 278 K, 600 MHz. For the amino protons, cross-peaks are labeled according to their assignments. In the base to H1′ region, the intraresidue H6/H8-H1′ cross-peaks are labeled with their residue numbers.

Hydration of [d(CGC)r($a_m a_m a_m$)d(TTTGCG)]$_2$

The qualitative and quantitative water hydration residence time can be determined by the cross-relaxation rate constants using NOESY and ROESY spectra (Hsu et al., 2000b; Lane et al., 1997; Otting et al., 1991). Previously, long-lived water molecules (correlation time $\tau_c > 0.3$ ns), with opposite signs of NOE and ROE, were found close to all H2 and H1′ protons of the RNA adenines of [d(CGC)r(aaa)d(TTTGCG)]$_2$ (Hsu et al., 2000b). Similar water-H1′ cross-peaks in RNA were also observed previously (Conte et al., 1996). The methyl group of 7T in [d(CGC)r(aaa)d(TTTGCG)]$_2$ also exhibited a positive NOE to water at 273 K, i.e., with a water correlation time longer than 0.3 ns. However, no such long-lived water molecules were found for the H2 and H1′ protons of the 2′-O-methylated RNA adenines or for the methyl group of 7T in [d(CGC)r($a_m a_m a_m$)d(TTTGCG)]$_2$ (Figure 1). This result is probably due to the hydrophobic enviroment

Table 3. Helical parameters for [d(CGC)r($a_m a_m a_m$)d(TTTGCG)]$_2$

Base	X disp (Å)	Buckle (°)	Pr. twist (°)	Incl. (°)	Twist (°)	Rise (Å)
1C	-3.0 ± 0.5	-3.1 ± 3.6	-9.0 ± 3.8	-1.8 ± 3.7	30.9 ± 2.3	3.4 ± 0.2
2G	-2.7 ± 0.6	-10.1 ± 3.1	-8.1 ± 2.3	-2.7 ± 3.4	33.7 ± 1.7	3.2 ± 0.2
3C	-3.0 ± 0.5	-2.9 ± 3.5	-3.5 ± 2.2	-5.5 ± 3.4	17.8 ± 1.7	3.7 ± 0.3
4a_m	-2.9 ± 0.4	-2.9 ± 2.4	-8.8 ± 5.8	-3.8 ± 3.2	27.6 ± 0.8	3.1 ± 0.1
5a_m	-2.7 ± 0.4	17.3 ± 3.3	-19.4 ± 3.2	6.5 ± 2.8	28.1 ± 1.1	4.9 ± 0.3
6a_m	-2.5 ± 0.3	-10.1 ± 2.2	-19.3 ± 1.5	8.5 ± 2.5	35.6 ± 0.5	2.7 ± 0.06
7T	-2.5 ± 0.3	7.5 ± 1.9	-18.9 ± 1.8	8.7 ± 2.5	27.4 ± 1.6	4.3 ± 0.4
8T	-2.7 ± 0.4	-11.3 ± 4.5	-24.8 ± 3.2	8.3 ± 3.2	29.3 ± 1.3	3.0 ± 0.1
9T	-2.8 ± 0.5	7.7 ± 4.1	-17.4 ± 7.8	-1.1 ± 4.5	16.7 ± 1.5	3.7 ± 0.4
10G	-3.0 ± 0.5	4.4 ± 3.6	-2.9 ± 3.0	-4.4 ± 4.8	31.5 ± 2.1	3.2 ± 0.1
11C	-2.7 ± 0.7	10.3 ± 3.0	-8.3 ± 3.4	-1.6 ± 4.8	31.3 ± 3.9	3.5 ± 0.2
12G	-2.9 ± 0.6	3.6 ± 6.4	-10.7 ± 5.0	-0.4 ± 4.6	–	–
Average	-2.8 ± 0.5	0.8 ± 3.5	-12.6 ± 3.6	0.9 ± 3.6	28.2 ± 1.7	3.5 ± 0.2
a3T3	-1.8 ± 0.1	-0.4 ± 3.6	-19.9 ± 2.1	-1.3 ± 1.4	32.7 ± 1.9	3.1 ± 0.2
A3T3	-0.3 ± 0.3	1.0 ± 7.4	-16.0 ± 11.0	0.7 ± 3.2	36.0 ± 4.2	3.4 ± 0.2
A3U3	-4.8 ± 0.1	1.8 ± 5.2	-24.7 ± 4.0	10.7 ± 4.9	32.3 ± 1.8	2.7 ± 0.4
A-RNA	−5.3	0.0	14.4	15.9	31.5	3.5
A-DNA	−5.4	0.0	13.7	19.1	30.9	3.4
B-DNA	−0.7	0.0	3.7	−5.9	36.0	3.4

[1]Helical parameters were calculated using the program Curves v. 5.2.
[2]a3T3 represents [d(CGC)r(aaa)d(TTTGCG)]$_2$, A3T3 represents [d(CGCAAATTTGCG)]$_2$, A3U3 represents [r(cgcaaauuugcg)]$_2$, and A-DNA, B-DNA, A-RNA represent the standard A- and B-form DNA and A-form RNA.

created by the 2′-O-methyl groups of the three 2′-O-methylated RNA adenines in the minor groove.

Orientation of 2′-O-methyl protons

NMR and X-ray studies of DNA•RNA hybrid and chimeric duplexes with 2′-O-methylated ribonucleotide insersions indicated that the 2′-O-methyl groups had the orientation with the gauche(+) torsion angles near 60° (Blommers et al., 1994; Lubini et al., 1994; Nishizaki et al., 1997). The gauche(+) orientations of 2′-O-methyl groups were attributed to that the C3′-endo sugar conformation pushing the bulky methyl group toward the minor groove and hence avoided contact with the opposite intraresidue 3′-phosphate group (Kawai et al., 1992; Nishizaki et al., 1997). According to an A-type helix model, the intranucleotide distances between the 2′-O-methyl group and the ribose protons with gauche(+) orientation can be calculated as follow: 2′-O-methyl group to H1′ proton is around 3 Å; 2′-O-methyl group to H2′ proton is less than 3Å; 2′-O-methyl group to H3′ proton is larger than 3.5 Å; and 2′-O-methyl group to H4′ proton is larger than 4 Å. Based on the observed NOE distances using the thymine H6-Me distance (2.9 Å) as a standard, 2′-O-methyl groups of 5a_m and 6a_m were found to orient toward the gauche(+) domain (Blommers et al., 1994; Lubini et al., 1994; Nishizaki et al., 1997). Surprisingly, this is not the case for 4a_m at the DNA•2′-OMe-RNA junction. The observed NOE intensity of 2′-O-methyl group to H1′ proton for 4a_m is much weaker than those of 5a_m and 6a_m (Figure 3). The 2′-O-methyl group of 4a_m was found to orient towards the trans domain with torsion angle near 180°. Such trans orientation was not observed in other DNA•RNA hybrid and chimeric duplexes with 2′-O-methylated RNAs (Blommers et al., 1994; Lubini et al., 1994; Nishizaki et al., 1997).

T_1 relaxation times of [d(CGC)r($a_m a_m a_m$)d(TTTGCG)]$_2$

T_1 relaxation times of the resolved protons of [d(CGC)r($a_m a_m a_m$)d(TTTGCG)]$_2$ were determined using the method described by Wang et al. (1992). T_1 values of the H2 protons of the 2′-*O*-methylated 4a_m and 5a_m were found to be 4.3 sec. T_1 values of 6a_m H2, 4a_m H8, and 5a_m H8 protons were found

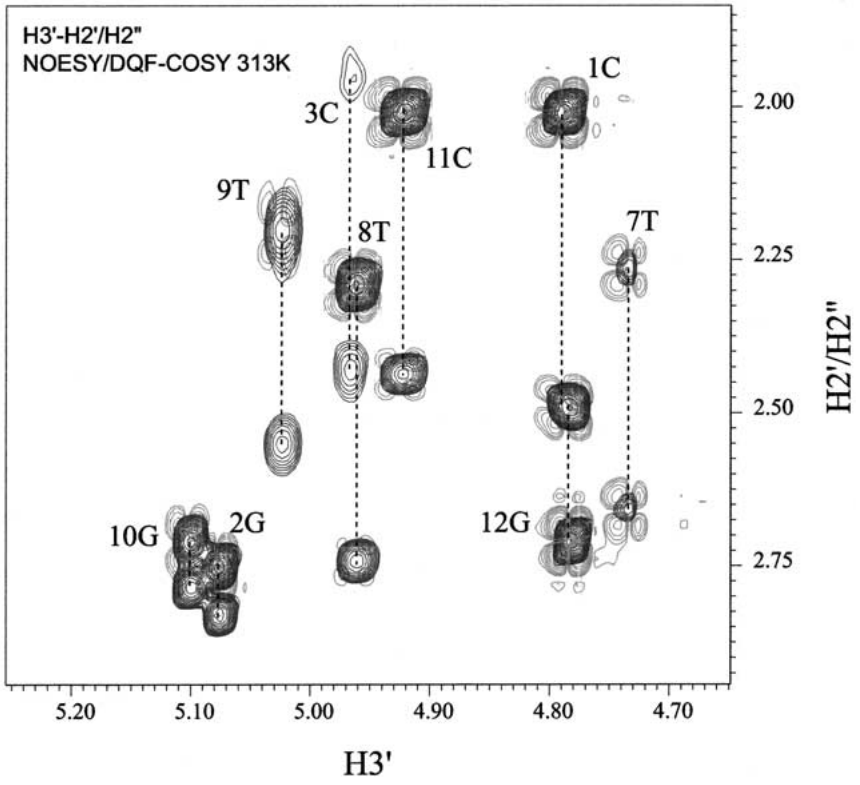

Figure 2. Expansion of the H2′/H2″-H3′ region of the overlapped NOESY (blue) and DQF-COSY (red) spectra of [d(CGC)r($a_m a_m a_m$)d(TTTGCG)]$_2$ showing the H2′/H2"-H3′ cross peak for DNA residue 7T. The other DNA residues, including residue 3C in the DNA-RNA junction, showed weak or no detectable H2″- H3′ DQF-COSY cross-peaks.

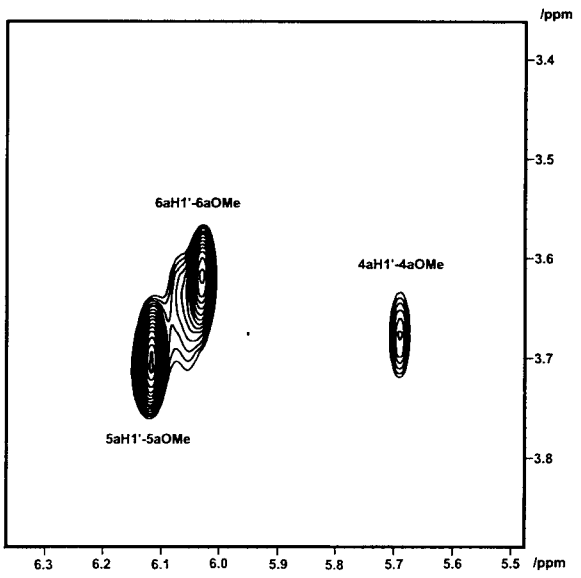

Figure 3. Expansion of the 2′-O-methyl group to H1′ region of the 120 ms NOESY spectrum of [d(CGC)r($a_m a_m a_m$)d(TTTGCG)]$_2$ collected at in D_2O at 303 K.

to be 3.6 sec. T_1 value of $6a_m$ H8 proton was found to be 2.9 sec. For the DNA aromatic and anometic protons, all T_1 values were found to be around 2.2 sec. Thus, the non-selective T_1 relaxation times for the aromatic protons of the 2′-*O*-methylated RNA adenines were ∼1.5–2 times longer than those of the DNAs in [d(CGC)r($a_m a_m a_m$)d(TTTGCG)]$_2$. As pointed out by Wang *et al.* (1992), for DNA•RNA chimeric duplexes, reliable distance data can be obtained from time-dependent NOESY data sets provided an adequately long relaxation delay is used. To avoid substantial errors due to the short relaxation delay, NOESY spectra were recorded at four different mixing times of 60, 120, 240 and 480 ms with a relaxation delay of 5 s at 303 K.

Structural features of [d(CGC)r($a_m a_m a_m$)d(TTTGCG)]$_2$

A total of ten final simulated annealing, restrained molecular dynamics, and NOE relaxation matrix refined structures (five from initial A-form and five from

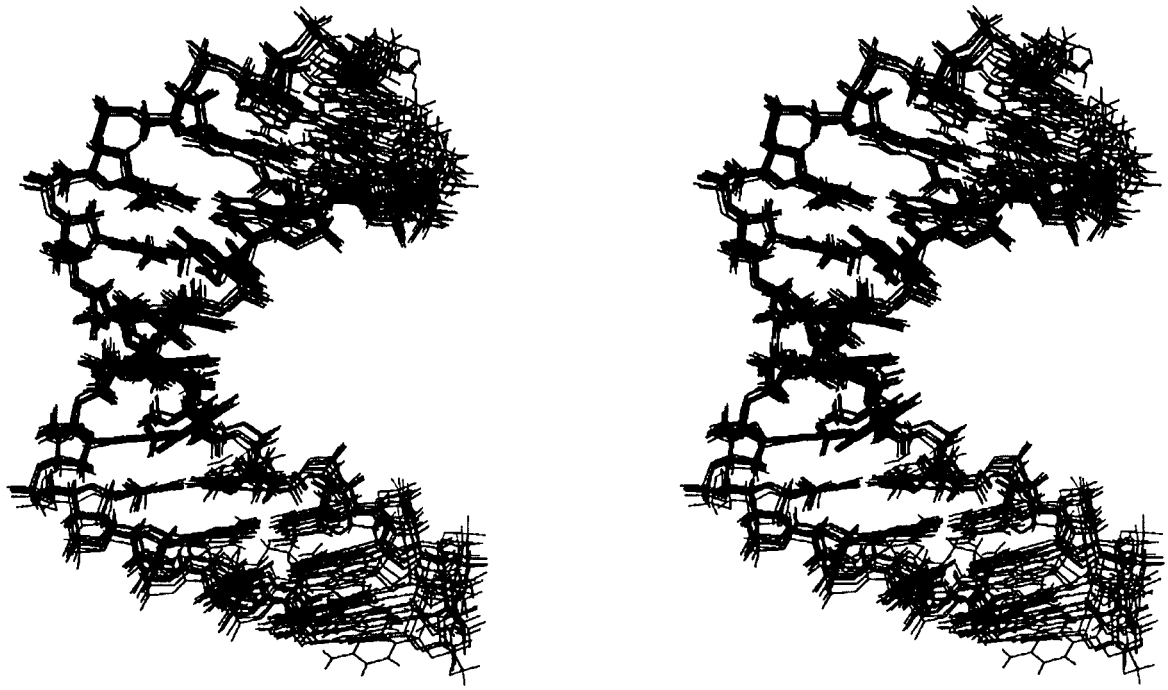

Figure 4. Stereoview of the superimposed ten final refined structures of [d(CGC)r($a_m a_m a_m$)d(TTTGCG)]$_2$.

initial B-form structures) were superimposed as shown in Figure 4. The energetic and geometric statistics of the ten best-refined structures are given in Table 1. The final ten structures superimposed well with a pairwise rmsd (heavy atoms) of 0.31 ± 0.12 Å for the hybrid segment and 1.12 ± 0.37 Å for the overall structures (Table 1). The average $R^{1/6}$ factor was 0.0268 ± 0.00026 which resembles well with the experimental data.

Previously, the X-ray structure of the DNA duplex, [d(CGCAAATTTGCG)]$_2$, was found to be of B-type (Edwards et al., 1992) and the structure of the RNA duplex, [r(cgcaaauuugcg)]$_2$, was determined to be an A-type by NMR spectroscopy (Conte et al., 1997). The solution conformation of the pure DNA•RNA chimeric duplex, [d(CGC)r(aaa)d(TTTGCG)]$_2$, was determined to be between it's A-RNA and B-DNA analogs (Hsu et al., 2000a). In comparison to its non-methylated analog, some of the local structural parameters of [d(CGC)r($a_m a_m a_m$)d(TTTGCG)]$_2$ were more similar to the A-type RNA duplex than to the pure DNA•RNA chimeric duplexe, particularly with respect to the minor groove width and the x-displacement (Figure 5A). The minor groove width in the central hybrid segment of [d(CGC)r($a_m a_m a_m$)d(TTTGCG)]$_2$ is close to the canonical A-RNA and A-DNA duplex (Figure 5A).

Figure 5B shows the sugar puckers for the final NMR refined solution structures compared to its DNA, RNA, and pure chimeric duplex analogs as well as standard B- and A-form DNA and A-form RNA. The sugar conformation of DNA residue 7T in the 2′-O-methylated-RNA-DNA junction was close to the O4′-endo range which was consistent with the spectral analysis. The sugar conformation of the rest of the DNA residues in this chimeric duplex are in the S-type range (C1′-exo to C2′-endo) while the 2′-O-methylated RNA residues are in the N-type range (C3′-endo). Other structural features (i.e. helical twists, X-displacement, rise, etc.) of [d(CGC)r($a_m a_m a_m$)d(TTTGCG)]$_2$ are shown in Table 3.

Discussion

The solution structure of [d(CGC)r($a_m a_m a_m$)d(TTTGCG)]$_2$ is different from either the uniformly A-type RNA duplex [r(cgcaaauuugcg)]$_2$in the solution state (Conte et al., 1997), or from the related B-type DNA duplex [d(CGCAAATTTGCG)]$_2$ in crystalline state (Edwards et al., 1992). The sugar conformation of

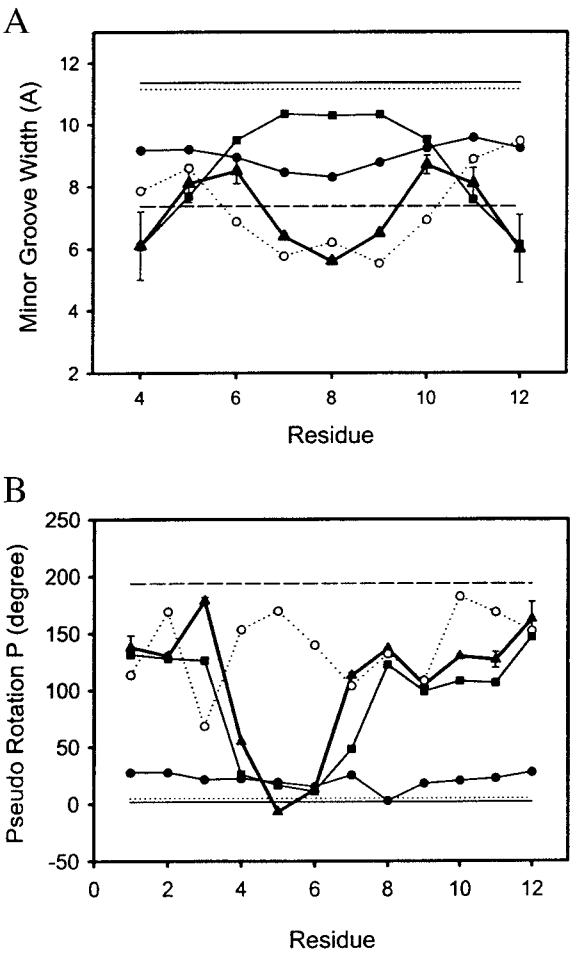

Figure 5. (A) Minor groove width as a function of position of the residue along the [d(CGC)r($a_m a_m a_m$)d(TTTGCG)]$_2$ duplex (—■—). The width is represented by the (n)P-(m+3)P phosphorus distance minus the phosphorus van der Waals radius of 5.8 Å. (B) Pseudo rotational phase angles (P) in the 10 final refined structures (—■—). The corresponding values for the pure DNA•RNA hybrid chimeric duplex [d(CGC)r(aaa)d(TTTGCG)]$_2$ (—▲—) and its X-ray derived B-DNA (.○.) and NMR derived A-RNA (—●—) analogs and for B-DNA (— —), A-DNA (. . .), and A-RNA (—) are also plotted for comparison.

[d(CGC)r($a_m a_m a_m$)d(TTTGCG)]$_2$ exhibits properties of a chimeric mixture of A-form and B-form in solution, similar to its pure chimeric duplex as reported previously (Hsu et al., 2000a).

With respect to the hybrid junctions, only the 7T•18a_m (or the symmetrical 19T•6a_m) DNA base pair in the hybrid junction is involved in the structural transition. Sugar conformation of 7T (19T) was found to be in the O4′-endo conformation based on both NOESY and DQF-COSY spectra (Figure 2). Sugar conformation of DNA residue 3C (15C) in the DNA duplex-hybrid duplex junction was found to be in the normal C1′-exo to C2′-endo conformation (Figure 5B). Thus, structural parameters of DNA residue at 5′-end of a DNA-hybrid junction are not affected by the A-type 2′-O-methylated RNA at 3′-end. Instead, changes in the structural parameters were observed for DNA residue at 3′-end of a hybrid junction by the A-type 2′-O-methylated RNA at 5′-end. This influence was involved in only one step.

Based on NOE distances, the torsion angle of the 2′-O-methyl group of 4a_m was found to be in the trans domain whereas it is in the gauche (+) domain for 5a_m and 6a_m. The energy minimization study of the 2′-O-methyl group in mononucleotide showed that there are two stable orientations for the RNA 2′-O-methyl group, with torsion angles around 180° and 72° (Kawai et al., 1992). Our result provides the first evidence that, at the DNA•2′-OMe-RNA junction, the 2′-O-methyl group orients toward the trans domain. Nevertheless, the 2′-O-methyl groups of 4a_m, 5a_m, and 6a_m with trans or gauche (+) orientations, all point to the minor groove of the duplex.

The width of the minor groove is an important structural parameter for DNA•RNA hybrid and chimeric duplexes. Previous studies have shown that the minor groove width of the DNA•RNA hybrid and chimeric duplex [d(CGC)r(aaa)d(TTTGCG)]$_2$ was found to be closer to the B-DNA analog than to the A-RNA duplex and may be responsible for the recognition and cleavage activity by RNase H (Hsu et al., 2000a). In the present study we have observed that the minor groove width of [d(CGC)r($a_m a_m a_m$)d(TTTGCG)]$_2$ was closer to the canonical A-RNA and A-DNA (Figure 5A). This may be due to the steric effect of the bulky 2′-O-methyl groups in the minor groove.

It was proposed that the incorporation of 2′-O-methyl ribonucleotide into DNA increases the melting temperature of the corresponding DNA•RNA duplexes by 0.8–1.4 °C per modification (Tereshko et al., 1998). The increased stability of the DNA•RNA chimeric duplex was attributed to the hydrophobic interactions between substituents in the minor groove (Lubini et al., 1994). To test if the 2′-O-methyl modification does increase the stability of the DNA•RNA chimeric duplex in our case, we have studied the thermal stability of [d(CGC)r($a_m a_m a_m$)d(TTTGCG)]$_2$ (Figure 6). Indeed, the 2′-O-methylation of riboadenines in pure chimeric dulpex increses its melting temperature from 48.5 °C to 51.9 °C, which is consistent with the previous report (Tereshko et al., 1998).

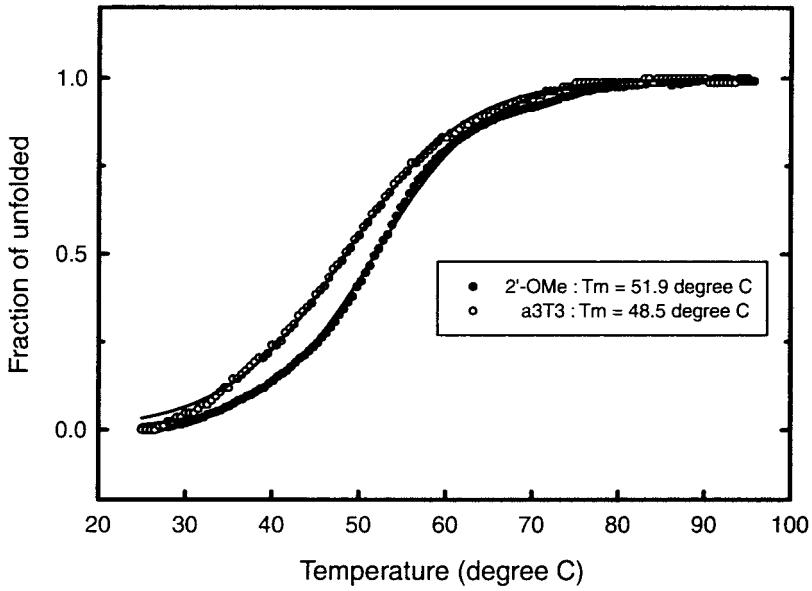

Figure 6. UV melting curve analysis of [d(CGC)r($a_m a_m a_m$)d(TTTGCG)]$_2$ (2′-OMe) and [d(CGC)r(aaa)d(TTTGCG)]$_2$ (a3T3).

Since no long-lived water molecules with correlation time τ_c larger than 0.3 ns were found close to the 2′-O-methylated RNA adenine H2 and H1′ protons in the hybrid segment and in the methyl group of 7T in the RNA-DNA junction, as observed in the case of the pure chimeric duplex (Hsu et al., 2000a, b), the increase in melting temperature may be due to the hydrophobic interactions between substituents in the minor groove (Lubini et al., 1994). Thus, if certain 2′-O-alkoxyalkyl substituents can be incorporated into the RNA residues to stabilize their hydration patterns, it may result in higher stability and nuclease resistance due to their hydrophobic interactions and the hydration patterns. This hypothesis was confirmed by the two recent X-ray structural studies of MOE (2′-O-methoxyethyl) and TOE (2′-O-methyl[tri-(oxyethyl)]) modified DNA•RNA hybrid and chimeric duplexes (Teplova et al., 1999; Tereshko et al., 1998). Extensive bound water molecules and hydrogen bonds were found in the MOE, TOE groups and in the nucleotide backbones. Both of the 2′-MOE and 2′-TOE modified DNA•RNA chimeric duplexes were found to have higher stability than the 2′-O-methyl modified chimeric duplex (Tereshko et al., 1998).

In conclusion, we have determined the solution structure of [d(CGC)r($a_m a_m a_m$)d(TTTGCG)]$_2$, where the central RNA adenines were substituted by 2′-O-methylated RNA adenines. The characteristic structural features of this chimeric duplex provide a basis for further understanding the possible therapeutic applications of DNA•RNA hybrid and chimeric duplexes with 2′-modified RNA residues.

Acknowledgements

This study was carried out on the 600 MHz NMR spectrometer at the Regional Instrument Center at Hsinchu, National Science Council, Taiwan, Republic of China. We thank the National Science Council of the Republic of China for research grants.

References

Ban, C., Ramakrishnan, B. and Sundaralingam, M. (1994) *J. Mol. Biol.*, **236**, 275–285.

Blommers, M.J.J., Pieles, U. and Mesmaeker, A.D. (1994) *Nucl. Acids Res.*, **22**, 4187–4194.

Cheng, J.-W., Chou, S.-H., Salazar, M. and Reid, B.R. (1992) *J. Mol. Biol.*, **228**, 118–137.

Chou, S.-H., Flynn, P. and Reid, B.R. (1989) *Biochemistry*, **28**, 2422–2435.

Conte, M.R., Conn, G.L., Brown, T. and Lane, A.N. (1996) *Nucl. Acids Res.*, **24**, 3693–3699.

Conte, M.R., Conn, G.L., Brown, T. and Lane, A.N. (1997) *Nucl. Acids Res.*, **25**, 2627–2634.

Edwards, K.J., Brown, D.G., Spink, N., Skelly, J.V. and Neidle, S. (1992) *J. Mol. Biol.*, **226**, 1161–1173.

Egli, M. and Gryaznov, S.M. (2000) *Cell. Mol. Life Sci.*, **57**, 1440–1456.

Fedoroff, O.Y., Salazar, M. and Reid, B.R. (1993) *J. Mol. Biol.*, **233**, 509–523.

Fedoroff, O.Y., Salazar, M. and Reid, B.R. (1996) *Biochemistry*, **35**, 11070–11080.
Gonzalez, C., Stec, W., Kobylanska, A., Hogrefe, R.I., Reynolds, M. and James, T.L. (1994) *Biochemistry*, **33**, 11062–11072.
Gonzalez, C., Stec, W., Reynolds, M.A. and James, T.L. (1995) *Biochemistry*, **34**, 4969–4982.
Gudima, S.O., Kazantseva, E.G., Kostyuk, D.A., Shchaveleva, I.L., Grishchenko, O.I., Memelova, L.V. and Kochetkov, S.N. (1997) *Nucl. Acids Res.*, **25**, 4614–4618.
Gyi, J.I., Lane, A.N., Conn, G.L. and Brown, T. (1998) *Biochemistry*, **37**, 73–80.
Hall, K.B. and McLaughlin, L.W. (1991) *Biochemistry*, **30**, 10606–10613.
Hare, D.R., Wemmer, D.E., Chou, S.-H., Drobny, G. and Reid, B.R. (1983) *J. Mol. Biol.*, **171**, 319–336.
Hashem, G.M., Pham, L., Vaughan, M.R. and Gray, D.M. (1998) *Biochemistry*, **37**, 61–72.
Hogrefe, H.H., Hogrefe, R.I., Walder, R.Y. and Walder, J.A. (1990) *J. Biol. Chem.*, **265**, 5561–5566.
Hsu, S.T., Chou, M.T. and Cheng, J.W. (2000a) *Nucl. Acids Res.*, **28**, 1322–1331.
Hsu, S.T., Chou, M.T., Chou, S.H., Huang, W.C. and Cheng, J.W. (2000b) *J. Mol. Biol.*, **295**, 1129–1137.
Jaishree, T.N., van der Marel, G.A., van Boom, J.H. and Wang, A.H.J. (1993) *Biochemistry*, **32**, 4903–4911.
Kawai, G., Yamamoto, Y., Kamimura, T., Masegi, T., Sekine, M., Hata, T., Iimori, T., Watanabe, T., Miyazawa, T. and Yokoyama, S. (1992) *Biochemistry*, **31**, 1040–1046.
Kim, S.-G., Lin, L.-J. and Reid, B.R. (1991) *Biochemistry*, **31**, 3564–3574.
Lane, A.N., Jenkins, T.C. and Frenkiel, T.A. (1997) *Biochim. Biophys. Acta*, **1350**, 205–220.
Lavery, R. and Sklenar, H. (1989) *J. Biomol. Struct. Dyn.*, **6**, 655–667.
Lubini, P., Zurcher, W. and Egli, M. (1994) *Chem. Biol.*, **1**, 39–45.
Nilges, M., Habazettl, J., Brunger, A.T. and Holak, T.A. (1991) *J. Mol. Biol.*, **219**, 499–510.
Nishizaki, T., Iwai, S., Ohkubo, T., Kojima, C., Nakamura, H., Kyogoku, Y. and Ohtsuka, E. (1996) *Biochemistry*, **35**, 4016–4025.
Nishizaki, T., Iwai, S., Ohtsuka, E. and Nakamura, H. (1997) *Biochemistry*, **36**, 2577–2585.
Noggle, J.H. and Schirmer, R.E. (1971) *The Nuclear Overhauser Effect*, Academic Press, New York, NY.
Otting, G., Liepinsh, E. and Wüthrich, K. (1991) *Science*, **254**, 974–980.
Piotto, M., Saudek, V. and Sklenar, V. (1992) *J. Biomol. NMR*, **2**, 661–665.
Ratmeyer, L., Vinayak, R., Zhong, Y.Y., Zon, G. and Wilson, W.D. (1994) *Biochemistry*, **33**, 5298–5304.
Rice, J. and Gao, X. (1997) *Biochemistry*, **36**, 399–411.
Salazar, M., Champoux, J.J. and Reid, B.R. (1993a) *Biochemistry*, **32**, 739–744.
Salazar, M., Fedoroff, O.Y., Miller, J.M., Ribeiro, N.S. and Reid, B.R. (1993b) *Biochemistry*, **32**, 4207–4215.
Salazar, M., Fedoroff, O.Y. and Reid, B.R. (1996) *Biochemistry*, **35**, 8126–8135.
Salazar, M., Fedoroff, O.Y., Zhu, L. and Reid, B.R. (1994) *J. Mol. Biol.*, **241**, 440–455.
Szyperski, T., Gotte, M., Billeter, M., Perola, E., Cellai, L., Heumann, H. and Wuthrich, K. (1999) *J. Biomol. NMR*, **13**, 343–355.
Teplova, M., Minasov, G., Tereshko, V., Inamati, G.B., Cook, P.D., Manoharan, M. and Egli, M. (1999) *Nat. Struct. Biol.*, **6**, 535–539.
Tereshko, V., Portmann, S., Tay, E.C., Martin, P., Natt, F., Altmann, K. and Egli, E. (1998) *Biochemistry*, **37**, 10626–10634.
Wang, A.C., Kim, S.G., Flynn, P.F., Chou, S.H., Orban, J. and Reid, B.R. (1992) *Biochemistry*, **31**, 3940–3946.
Wang, A.H.-J., Fujii, S., van Boom, J.H., van der Marel, G.A., van Boeckel, S.A.A. and Rich, A. (1982) *Nature*, **299**, 601–604.
White, S.A., Nilges, M., Huang, A. and Brunger, A.T. (1992) *Biochemistry*, **31**, 1610–1621.
Wüthrich, K. (1986). *NMR of Proteins and Nucleic Acids*. John Wiley and Sons, New York, NY.
Yip, P. and Case, D.A. (1989) *J. Magn. Reson.*, **83**, 643–648.
Zhu, L., Salazar, M. and Reid, B.R. (1995) *Biochemistry*, **34**, 2372–2380.